CARDIAC

Quantification of global myocardial function by cine MRI deformable registration-based analysis: Comparison with MR feature tracking and speckle-tracking echocardiography

Mariana M. Lamacie[1] · Paaladinesh Thavendiranathan[1,2] · Kate Hanneman[1,3] ·
Andreas Greiser[4] · Marie-Pierre Jolly[5] · Richard Ward[2] · Bernd J. Wintersperger[1,3,6]

Abstract

Objectives To evaluate deformable registration algorithms (DRA)-based quantification of cine steady-state free-precession (SSFP) for myocardial strain assessment in comparison with feature-tracking (FT) and speckle-tracking echocardiography (STE).

Methods Data sets of 28 patients/10 volunteers, undergoing same-day 1.5T cardiac MRI and echocardiography were included. LV global longitudinal (GLS), circumferential (GCS) and radial (GRS) peak systolic strain were assessed on cine SSFP data using commercially available FT algorithms and prototype DRA-based algorithms. STE was applied as standard of reference for accuracy, precision and intra-/interobserver reproducibility testing.

Results DRA showed narrower limits of agreement compared to STE for GLS (-4.0 [-0.9,-7.9]) and GCS (-5.1 [1.1,-11.2])

than FT (3.2 [11.2,-4.9]; 3.8 [13.9,-6.3], respectively). While both DRA and FT demonstrated significant differences to STE for GLS and GCS (all p<0.001), only DRA correlated significantly to STE for GLS (r=0.47; p=0.006). However, good correlation was demonstrated between MR techniques (GLS:r=0.74; GCS:r=0.80; GRS:r=0.45, all p<0.05). Comparing DRA with FT, intra-/interobserver coefficient of variance was lower (1.6 %/3.2 % vs. 6.4 %/5.7 %) and intraclass-correlation coefficient was higher. DRA GCS and GRS data presented zero variability for repeated observations.

Conclusions DRA is an automated method that allows myocardial deformation assessment with superior reproducibility compared to FT.

Key Points
- *Inverse deformable registration algorithms (DRA) allow myocardial strain analysis on cine MRI.*
- *Inverse DRA demonstrated superior reproducibility compared to feature-tracking (FT) methods.*
- *Cine MR DRA and FT analysis demonstrate differences to speckle-tracking echocardiography*
- *DRA demonstrated better correlation with STE than FT for MR-derived global strain data.*

✉ Bernd J. Wintersperger
Bernd.Wintersperger@uhn.ca

1 Department of Medical Imaging, University Health Network, Toronto, Ontario, Canada

2 Department of Medicine, Division of Cardiology, University of Toronto, Toronto, Ontario, Canada

3 Department of Medical Imaging, University of Toronto, Toronto, Ontario, Canada

4 Siemens Healthcare, Erlangen, Germany

5 Siemens Healthcare, Medical Imaging Technologies, Princeton, NJ, USA

6 Department of Medical Imaging, Toronto General Hospital, 1 PMB-273, 585 University Avenue, Toronto, Ontario M5G 2N2, Canada

Introduction

Cardiovascular disease is the main cause of morbidity and mortality worldwide with a lifetime risk of heart failure at age 40 years of one in five [1–3]. Assessment of left ventricular (LV) ejection fraction (EF) as a measure of global systolic function is frequently performed in the evaluation of cardiac

pathology and has prognostic value [4, 5]. Cardiac magnetic resonance imaging (MRI) is considered the reference standard for the assessment of ventricular volumes and global systolic function due to its high reproducibility and low variability [6]. However, changes in global systolic function as measured by LVEF may occur late after onset of cardiac pathology [7]. Evaluation of myocardial deformation is more sensitive for detecting early cardiac disease [8, 9].

Cardiac MRI is also considered the standard in analysis of regional and global myocardial deformation, referred to as myocardial strain [10]. Cardiac MRI-measured myocardial strain is highly reproducible and accurate [11–13]. However, strain assessment often requires dedicated imaging techniques with advanced processing such as myocardial tissue tagging, strain encoded (SENC) MRI and displacement encoding with stimulated echoes (DENSE) MRI [11, 14–16]. For that reason, such techniques are commonly applied in research settings but rarely used in routine clinical practice. The application of feature-tracking (FT) algorithms derived from echocardiography to cine steady-state free-precession (SSFP) MRI data has been proposed for analysis of regional myocardial deformation [17–19]. Such approaches can be applied retrospectively to clinically acquired cine SSFP in order to obtain quantitative measures of regional myocardial motion, hence eliminating the need for separate acquisitions [20, 21]. These algorithms are derived from optical flow tracking techniques and follow each limited point from manually contoured endo- and epicardial borders (on a single frame) over time [19, 20].

Efforts in quantitative myocardial assessment have most recently expanded the use of algorithms that provide motion correction on acquisitions such as myocardial perfusion and myocardial mapping techniques [22–24]. Such algorithms perform calculation of deformation maps on a pixel basis for non-rigid image registration. Applied in a reverse fashion such algorithms can be used for deformable registration-based analysis (DRA) of cine cardiac MRI in order to quantify regional myocardial motion [25–27].

We hypothesize that DRA algorithms allow for accurate and reproducible analysis of myocardial strain based on cine SSFP MRI. The aim of this study therefore was to compare DRA algorithms with FT cine MR analysis of cine SSFP data sets using speckle-tracking echocardiography (STE).

Materials and methods

Study population

Imaging data were acquired as part of the 'MR Imaging of Diffuse Myocardial Fibrosis in Transfusion-Dependent Anemias (MAFIO)' trial (Clinicaltrials.gov, NCT02090699). This study recruited 31 patients with thalassemia major and 10 age- and gender-balanced healthy controls [28]. For the current study, data sets of three patients (significant arrhythmia; situs inversus; data corruption during upload) were excluded during initial data review due to segmentation failure of the DRA prototype software. In 28 patients (34.7±9.6 years, 57.1 % male) and 10 healthy controls (31.5±4.4 years, 50.0 % male) all MR and echo data required for comparison was available and included into the analysis. Relevant study population details are outlined in Table 1. The study was approved by the local research ethics board and written informed consent was obtained from all subjects. All study participants underwent cardiac MR imaging and echocardiography on the same day (<6 h).

Table 1 Patient demographics and characteristics

	Patients (n=28)	Volunteers (n=10)	Total (n=38)
Age (years)	34.7 ± 9.6	31.5 ± 4.4	33.8 ± 8.6
Sex (male)[*]	57.1 % (n=16)	50.0 % (n=5)	55.3 % (n=21)
Previous iron overload[*]	60.7 % (n=17)	n.a.	n.a.
Current chelation therapy	100.0 % (n=28)	n.a.	n.a.
LV parameters[#]			
Ejection fraction (%)	60.7 ± 6.1	60.1 ± 3.1	60.5 ± 5.4
End-diastolic Volume (ml/m^2)	89.1 ± 17.9	99.8 ± 15.3	91.9 ± 17.7
Haemodynamics in echo			
Heart rate (bpm)	72.5 ± 12.3	65.6 ± 13.0	69.0 ± 12.7
Systolic blood pressure (mmHg)	98.7 ± 11.8	108.4 ± 13.6	101.3 ± 12.9
Rate pressure product	7,088.2 ± 1,123.6	6,380.8 ± 1,063.0	6,897.0 ± 1,138.3
Haemodynamics in MRI			
Heart rate (bpm)	73.0 ± 10.7	59.1 ± 8.1	71.3 ± 11.4
Systolic blood pressure (mmHg)	121.7 ± 15.1	120.7 ± 23.8	121.5 ± 17.0
Rate pressure product	8,969.9 ± 1,740.3	7,970.3 ± 2,418.2	8,728.6 ± 1,927.2

[*] defined by T2* <20ms; [#] by cine MR

Magnetic resonance imaging

Cardiac MRI examinations were performed at 1.5T (MAGNETOM Avanto fit, Siemens Healthcare GmbH, Erlangen, Germany) employing dedicated coil arrays. Cine SSFP imaging was performed using retrospective ECG-gating with acquisition of three LV long axis orientations (2-, 3-, 4-chamber) as well as a stack of short axis slices for LV coverage. Cine SSFP acquisitions were performed with 6-mm slice thickness (2-mm gap for short axis) and a pixel size of 1.4–1.6x1.4-1.6 mm (GRAPPA R=2). With the acquisition of 11 lines/segment (TR/TE:3/1.3ms) a temporal resolution of 33 ms was achieved with subsequent reconstruction of 25 phases/RR interval.

Echocardiographic acquisition

In all patients transthoracic echocardiography was performed by research sonographers using commercially available equipment (E9/Vivid 7, GE Healthcare, Milwaukee, WI, USA) following American Society of Echocardiography (ASE) recommendations [29]. Additional high frame rate acquisitions (>50 frames/s) were obtained in 2-, 3- and 4-chamber and mid short axis orientation (at level of papillary muscles) for subsequent strain analysis. All echo data were stored in the raw data format for subsequent analysis.

Image processing

Echocardiography and cardiac MR data were analysed for principal myocardial strain (Fig. 1). Analysis was performed on all available long axes orientations in both modalities as well as a single mid-ventricular short axis location. To ensure comparable short axis slice locations for both echocardiography and MRI data, two readers selected the appropriate mid-ventricular slice based on a comparative review of anatomical features (LV/RV trabeculations, moderator band and papillary muscles) in a consensus setting. Subsequently data were assessed for longitudinal strain (E_{ll}) as well as circumferential (E_{cc}) and radial (E_{rr}) strain. Peak systolic global longitudinal strain (GLS), global circumferential strain (GCS) and global radial strain (GRS) data are reported for both modalities using Lagrangian strain priniciples.

Magnetic resonance imaging data analysis

Cine SSFP-based peak systolic strain measurements in all subjects were analysed by two different post-processing approaches using FT analysis and deformable registration analysis (DRA).

GLS values for both cine SSFP approaches were based on calculation of the mean of the peak systolic GLS results for the individual long axis orientations.

In order to assess for intra-observer variability, a single observer (M.M.L.) performed repeated analysis of all MRI data with a minimal interval of 2 weeks and blinded to results of the initial measurements. To assess for interobserver variability, all datasets were analysed by a second experienced observer (B.J.W.).

MR feature-tracking

Feature-tracking analysis was performed using commercially available software algorithms (2D Cardiac Performance Analysis MR, Tomtec, Germany) on a dedicated off-line workstation [19]. Following data import, the endocardial border was drawn manually on an end-diastolic frame of all three long axes and the selected single short axis image. The drawn contour was subsequently projected and tracked on consecutive frames of cine SSFP series by the FT algorithm. In case of incorrect endocardial contour tracking, the observer corrected contours on both end-diastolic and end-systolic frames for a maximum of three times after which the generated contours were accepted. After observer contour approval, strain data and curves including peak systolic strain were generated and results exported.
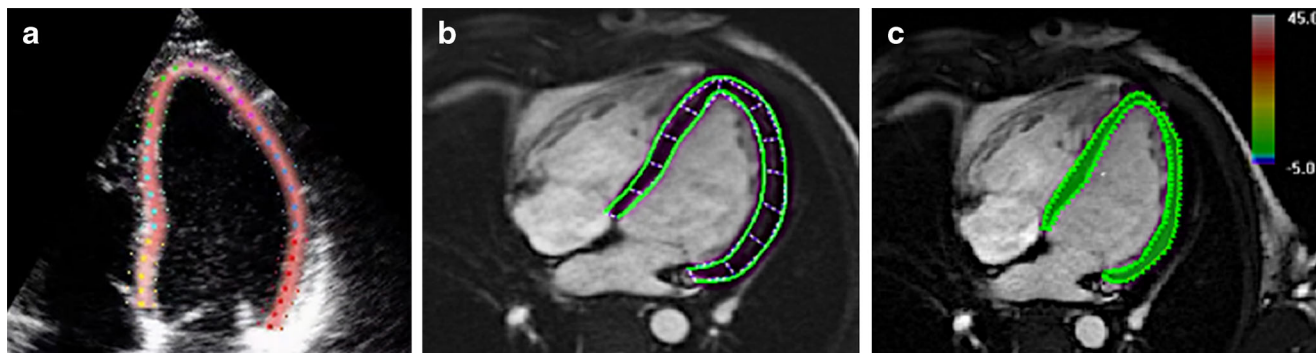

Fig. 1 The three methods used for strain analysis represented in a four-chamber (identical patient) view after segmentation being (**a**) speckle-tracking echocardiography (STE), (**b**) feature-tracking (FT) and (**c**) deformable registration analysis (DRA)

MR deformable registration analysis

Inverse DRA was performed using a prototype automated segmentation tool programmed in Visual C++ (Trufi Strain, Siemens Healthcare, Medical Imaging Technologies, Princeton, NJ, USA). The software automatically identifies anatomical landmarks such as the mitral valve points and apex point on long axis slices and the RV insertion points and lateral point on short axis images. The software subsequently automatically delineates endo- and epicardial myocardial borders on short axis data sets [26, 30]. In order to ensure temporal consistency of the endo- and epicardial contours, the segmentation algorithm relies on a deformable registration algorithm that calculates dense deformation fields between any two frames in a slice. After a contour is identified in one frame, it is automatically propagated to the other frames in the slice [27].

Analysis of long axis strain followed a semi-automated approach with the observer drawing an initial endocardial and epicardial contour on diastolic frames of all three available long axis orientations without further corrections. Processing was then automatically performed with propagation of these contours to all other frames using the same deformable registration algorithm [27].

Deformation fields calculated for the purpose of contour segmentation can directly be used to calculate strain values inside the myocardium because the Lagrangian strain tensor can directly be expressed in term of the gradients of the displacement fields (online appendix) (Figs. 2 and 3). All results were exported for data analysis.

Echocardiography speckle-tracking analysis

Strain analysis was performed using a commercially available software package (EchoPAC, Version 112, GE Healthcare, Milwaukee, WI, USA) by an experienced physician (P.T.) blinded to all clinical data. After initial review of source data, strain analysis was only pursued in case of overall sufficient image quality.

Fig. 2 Deformable registration analysis (DRA)-based analysis of longitudinal strain on a (**a**) four-chamber view and (**b**) two-chamber view cine steady-state free-precession (SSFP) data. (**c**) Resulting longitudinal strain curves over the cardiac cycle for individual 3-ch (cine SSFP not shown), 4-ch and 2-ch orientation with superimposed (*solid line*) global longitudinal strain curve
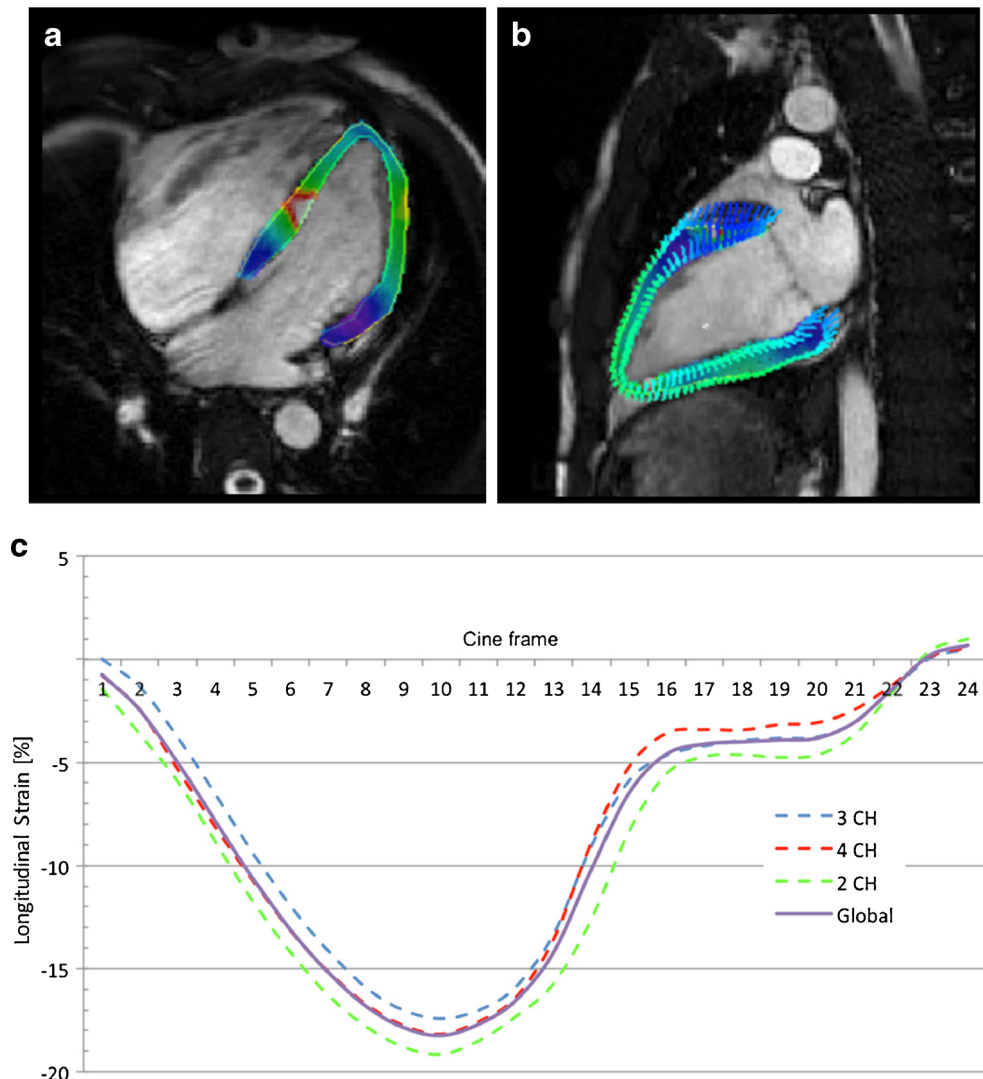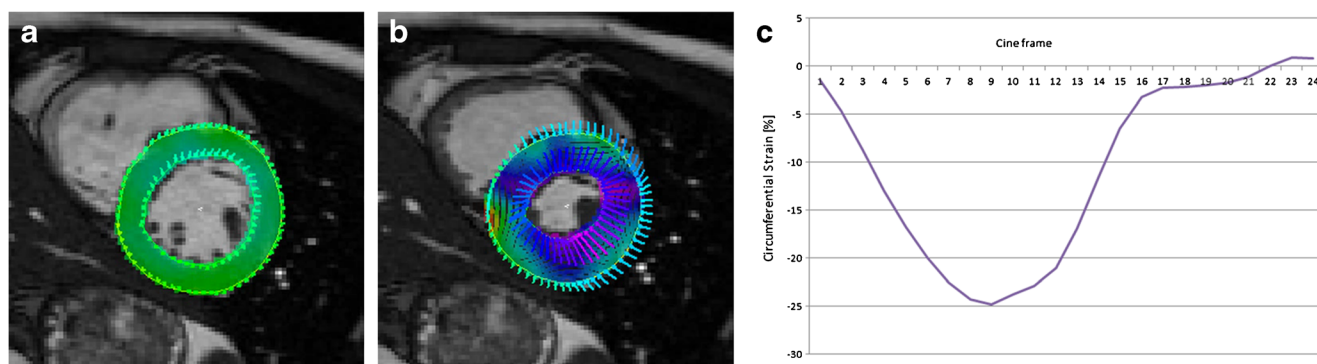
Fig. 3 Left mid-ventricular slice at (**a**) end-diastole and (**b**) end-systole with resulting (**c**) global circumferential strain curve during the cardiac cycle

Peak systolic global longitudinal strain (GLS) was measured using automated myocardial contours generated by placing three seed points on each of the three long axis views with subsequent automatic contour generation. Any contour adjustment was performed as necessary. However, after 3 attempts, poorly tracked segments were excluded. The GLS was calculated based on the average of the peak systolic global longitudinal strain from the three long axis orientations. Circumferential and radial strain analysis was performed on short axis slices obtained at the papillary muscle level (mid left ventricular level). For short axis analysis the entire endocardium had to be traced manually and adjusted as necessary. For radial and circumferential strain the peak systolic strain values for each of the six segments were averaged to obtain a measure of global strain for that slice.

Statistical analysis

Strain data are presented as mean ± SD and with strain values reported in percentages. Cardiac MR and echocardiography data were tested for normal distribution (D'Agostino-Pearson test) and subsequently compared using Student's t-test. In addition, Bland-Altman analysis, linear regression analysis and Spearman's correlation coefficient were used for method comparison. Analysis for potentially influential data points was perfomed extracting Cooks distance and leverage values. Thresholds for either value for exclusion were set to 4/n. Intra- and interobserver variability for repeated analysis of all MR data with MR feature-tracking and DRA were assessed with intra-class correlation (ICC) and coefficient of variation (COV) in addition to Bland-Altman analysis. For all statistical analysis MedCalc® (Version 15.2.2, MedCalc Software bvba, Ostend, Belgium) and SPSS (Version 23, IBM, New York, USA) was used. Statistical significance was defined as p < 0.05 and Bonferroni correction was applied for multiple pairwise comparisons as necessary.

Results

Speckle-tracking echocardiography strain evaluation was successful in 89 % (34/38) of subjects for global longitudinal

strain and 97 % (37/38) of all subjects for both radial and circumferential strain. The rest of the data was excluded due to poor image quality. In one patient a single segment was excluded from GLS computation but data were otherwise included. Both MR approaches allowed successful strain analysis of cine SSFP data for all data sets (100 %; 38/38).

Global longitudinal strain

GLS values for cine MR-based quantification were -23.2±3.9 % (95 % CI: -24.6, -21.8) by FT and -16.0±1.7 % (95 % CI: -16.5, -15.4) by DRA (P<0.0001). Comparison of both MRI approaches to STE-derived GLS data (-20±1.6 % [95 % CI: -20.5, -19.4]) demonstrated significant differences (both P<0.0001) (Table 2). Comparison with STE-derived data demonstrated narrower limits of agreement with a slightly higher mean bias for DRA (bias: -4.0, limits of agreement (LOA): -0.9,-7.9) than FT (bias: 3.2, LOA: 11.2,-4.9) (Table 3). Including all data points, GLS data generated by DRA (r=0.31,p=0.07) and FT (r=0.09,p=0.6) did not show significant correlation with STE results, while there was good correlation between both MR approaches (r=0.74, p<0.0001). Exclusion of the most influencial data points (n=2) as described resulted in significant correlation of DRA to STE (r=0.47, p=0.006) while no relevant change was identified for FT (r=0.25, p=0.16) (Fig. 4). Furthermore, FT- and DRA-derived GLS correlated signficiantly to LV EF (Table 4).

Global circumferential strain

MR-based GCS analysis demonstrated significant differences in pairwise comparisons to STE GCS data. FT-based GCS data were -28.3±4.9 % (95 % CI: -29.9, -26.7) (P<0.0001) while DRA-measured values were -19.4±2.6 % (95 %CI: -20.3, -18.6) (P<0.0001); both were different from STE-based data (-24.5±2.3 % (95 % CI: -25.2,-23.7) (Table 2). Comparison with STE-derived data demonstrated higher mean bias but narrower limits of agreement for DRA-(bias: -5.1, LOA: 1.1, -11.2) based GCS values than FT-based data

Table 2 Overview of results for global longitudinal (GLS), circumferential (GCS) and radial (GRS) strain values based on speckle-tracking echocardiography (STE), cine SSFP-based feature-tracking (FT) and inverse deformable registration analysis (DRA) techniques. Results are provided for the total cohort as well as for the patient and volunteer subgroups

		DRA			FT			STE		
		Mean (%)	SD	95 % CI	Mean (%)	SD	95 % CI	Mean (%)	SD	95 % CI
GLS	Total (n=34)	-16.0	1.7	-16.5,-15.4	-23.2	3.9	-24.6,-21.8	-20.0	1.6	-20.5,-19.4
	Patients (n=25)	-16.1	1.6	-16.8, -15.5	-24.1	3.7	-25.6, -22.5	-19.7	1.5	-20.3, -19.1
	Volunteers (n=9)	-15.6	2.1	-17.2, -14.0	-20.8	3.6	-23.6, -18.0	-20.8	1.8	-22.3, -19.4
GCS	Total (n=37)	-19.4	2.6	-20.3,-18.6	-28.3	4.9	-29.9,-26.7	-24.5	2.3	-25.2,-23.7
	Patients (n=28)	-19.5	2.7	-20.5, -18.4	-28.7	5.1	-30.6, -26.7	-24.5	2.3	-25.4, -23.6
	Volunteers (n=9)	-19.2	2.2	-20.9, -17.5	-27.2	4.5	-30.7, -23.7	-24.4	2.3	-26.1, -22.6
GRS	Total (n=37)	36.6	7.3	34.2,39.1	36.1	9.7	33.0,39.5	44.9	12.0	40.9,48.9
	Patients (n=28)	37.1	7.0	34.4, 39.8	37.6	10.5	33.5,41.6	45.9	12.0	41.2, 50.5
	Volunteers (n=9)	34.0	7.7	28.1, 39.9	31.6	5.9	27.1, 36.1	41.7	12.1	32.4, 51.1

For comparability reasons presented data is based on numbers of cases where data was availabile for all three techniques. No significant differences were found between patients and volunteers for any of the applied methods and parameters

(bias: 3.8, LOA: 13.9, -6.3) (Table 3). There was no significant correlation with STE for either DRA or FT (r=0.17, p=0.3 and r=0.13, p=0.4, respectively), but there was a good correlation between FT and DRA (r=0.8, p<0.0001) (Fig. 5). No influential data points were identified by further statistical analysis. FT- and DRA-derived GCS correlated signficiantly with LV EF (Table 4).

Global radial strain

No significant differences were found between FT- and DRA-based analysis of cine MR for GRS (p=0.79). However, results for both FT (36.1±9.7 % (95 % CI: 33.0, 39.5); p=0.0005) and DRA (36.6±7.3 % (95 % CI: 34.2, 39.1); p=0.0003) differed significantly from STE (44.9±12.0 % (95 %CI: 40.9, 48.9)) (Table 2). Bland-Altman plots demonstrated relatively wide limits of agreement with only minimal mean bias between both MR-based methods (bias: -0.4, LOA: 17.4, -18.2) while in comparison with STE both presented wide LOA and comparable bias (bias: 8.5, LOA: 34.1, -17.1 for DRA and bias: 8.8, LOA: 36.0, -18.4 for FT) (Table 3). Both DRA and FT demonstrated no significant correlation with STE (r=0.14, p=0.38 for DRA and r=0.19, p=0.24 for FT) and correlation was moderate between DRA and FT

Table 3 Bland-Altman results for the applied methods for global longitudinal (GLS), circumferential (GCS) and radial (GRS) strain

	STE vs. DRA	STE vs. FT	FT vs. DRA
GLS	-4.0 (-0.9, -7.9)	3.2 (11.2, -4.9)	-7.2 (-1.9, -12.5)
GCS	-5.1 (1.1, -11.2)	3.8 (13.9, -6.3)	-8.9 (-2.6, -15.2)
GRS	8.5 (34.1, -17.1)	8.8 (36.0,-18.4)	-0.4 (17.4, -18.2)

Values are bias with BA limits of agreement in parenthesis

(r=0.45, p=0.0038) (Fig. 6). Again, no specifically influencial data points were identified by further statistical analysis.

Intra-observer and inter-observer reproducibility

Intra-observer reproducibility (GLS)

Bland-Altman plots demonstrated narrower limits of agreement for DRA-derived GLS data with less scatter around the bias and fewer outliers (bias: 0.05, LOA: -0.67, 0.77 for DRA vs. bias: -0.38, LOA: -4.45, 3.67 for FT) (Fig. 7a). ICC for intra-observer analysis was higher for DRA (0.99, 95 % CI: 0.98, 0.99) in comparison with FT (0.91, 95 % CI: 0.84, 0.95). COV was lower for DRA (1.6 %) compared with FT (6.4 %) (Table 5).
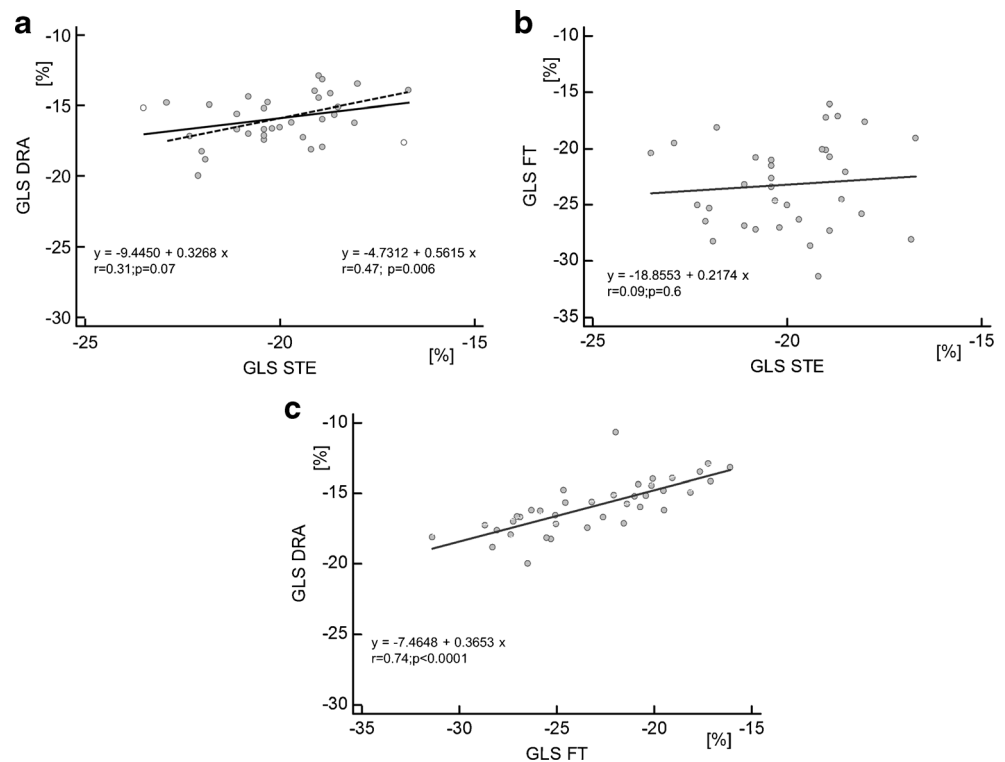
Interobserver reproducibility (GLS)

Agreement was better for DRA (bias: 0.45, LOA: -0.67, 1.57) than FT (bias: -0.03, LOA: -3.75, 3.68) (Fig. 7b). ICC was also higher for DRA (0.97, 95 % CI: 0.84, 0.98) in comparison with FT (0.92, 95 % CI: 0.86, 0.96) and COV was also lower for DRA (3.2 %) as compared to FT (5.7 %) (Table 5).

Intra-observer reproducibility (GCS, GRS)

Due to the fully automated contouring in DRA, ICC was 1.0 and COV was 0.0 for both GCS and GRS while with FT ICC and COV for GCS was 0.95 (95 % CI: 0.90, 0.97) and 5.2 % and for GRS was 0.91 (95 % CI: 0.82, 0.95) and 11.8 %, respectively (Table 5). On Bland-Altman plots, DRA analysis showed perfect agreement for GCS (Fig. 8a) and GRS while the variability for FT was larger (Table 5).

Fig. 4 Linear regression analysis for peak systolic GLS between all applied methods showing (**a**) results for speckle-tracking echocardiography (STE)-deformable registration analysis (DRA) comparison, (**b**) STE-feature-tracking (FT) comparison and (**c**) FT-DRA comparison. In (**a**) the dotted line shows regression after exclusion of influencial data points (*white data points*) as described

Interobserver reproducibility (GCS, GRS)

The interobserver analysis demonstrated ICC of 1.0 and COV of 0.0 for both GCS and GRS analysis with DRA. For FT, ICC and COV for GCS was 0.93 (95 % CI: 0.84, 0.96) and 6.1 % while for GRS was 0.72 (95 % CI: 0.47, 0.85) and 18.9 %, respectively (Table 5). On Bland-Altman plots, DRA data showed perfect agreement for GCS (Fig. 8b) and GRS while the variability with FT was higher (Table 5).

Discussion

Presented results demonstrate that the inverse application of DRA on routinely acquired cine SSFP data allows for assessment of global longitudinal, circumferential and radial myocardial strain. DRA provided lower variability for measurement of GLS and GCS than FT in comparison with speckle-tracking echocardiography. In addition, DRA analysis had

superior inter and intra-observer reproducibility compared to FT for all strain measurements. However, although there was good correlation between the MR-based techniques, the correlation with STE was limited, especially for FT analysis.

Although myocardial tagging is not commonly used in clinical practice due to its complexity and the need for dedicated acquisition/post-processing, its excellent reproducibility is among the reasons for MR tagging being considered the reference standard for evaluation of regional function, and as such also applied in various research and validation studies [20]. In a healthy population, MR tagging based normal values are approximately -15 %, -20 % and 35 % for GLS, GCS and GRS, respectively [31].

While in routine MRI quantitative analysis of regional function is rarely performed, echocardiography is, at present, increasingly being used for assessment of myocardial strain. This is partly driven by availability, the ease of acquisition and post-processing. With STE, the addition of longitudinal strain analysis to the evaluation of LVEF improves sensitivity for identifying subclinical disease in a large spectrum of cardiac disease [8, 9, 21, 32–34]. A meta-analysis by Yingchoncharoen et al. suggested that normal values for STE-measured GLS were between -15.9 % and -22.1 %, GCS between -20.9 % and -27.8 % and GRS between 35.1 % and 59 % [35]. However, there are inconsistent data on normal strain values by echocardiography due to variability between vendors and strain algorithms resulting in vendor-specific normal GLS ranges (between -17.3 % and o -21.5 %) within standard guidelines [29, 35, 36].

Table 4 Correlation between cardiac MR-derived left ventricular EF and GCS and GLS by both MR methods

Cardiac MR EF vs.		r	p
DRA	GLS	0.50	0.0014
	GCS	0.78	<0.0001
FT	GLS	0.52	0.0007
	GCS	0.67	<0.0001

p<0.05 was considered statistical significant

Fig. 5 Linear regression analysis for peak systolic GCS between all applied methods showing (**a**) results for speckle-tracking echocardiography (STE)-deformable registration analysis (DRA) comparison, (**b**) STE-feature-tracking (FT) comparison and (**c**) FT-DRA comparison
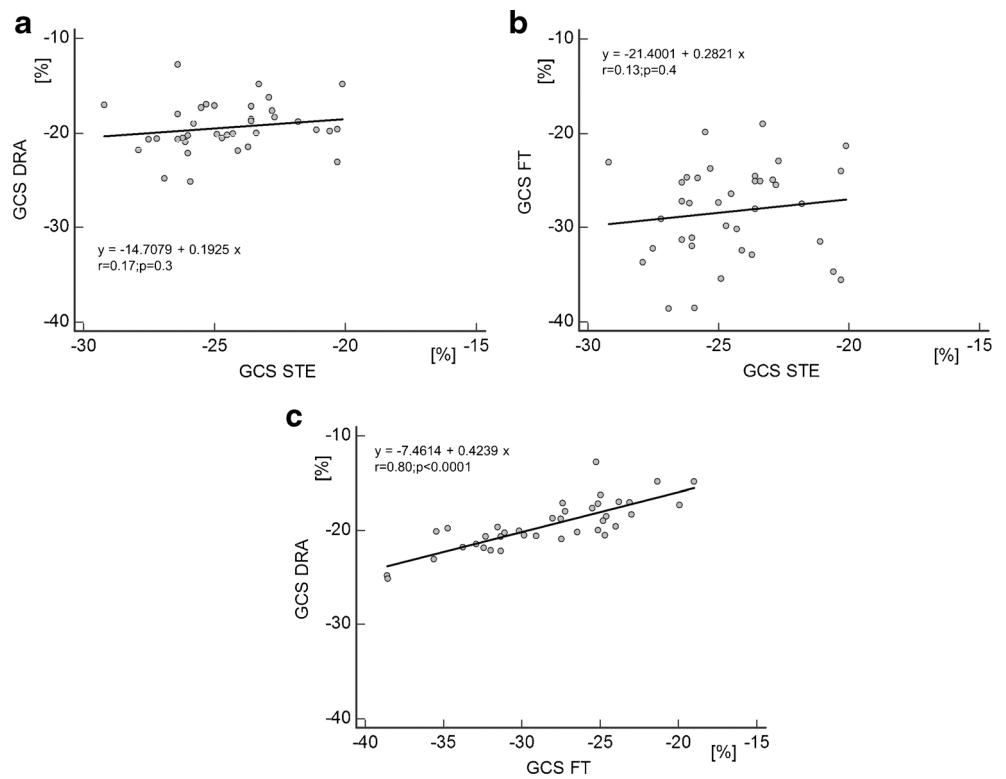
Modified FT algorithms, which are generally based on the principle of tissue voxel motion tracking, have recently gained attention for use on cine MRI. As such, regional myocardial motion can quantitatively be assessed on cine SSFP without the need for add-on acquisitions [20, 21]. These techniques have previously been compared to STE as well as MR tagging. Onishi et al. demonstrated good correlation with STE for GLS and GCS [21] and others have demonstrated reasonably

Fig. 6 Linear regression analysis for peak systolic GRS between all applied methods showing (**a**) results for speckle-tracking echocardiography (STE)-deformable registration analysis (DRA) comparison, (**b**) STE-feature-tracking (FT) comparison and (**c**) FT-DRA comparison
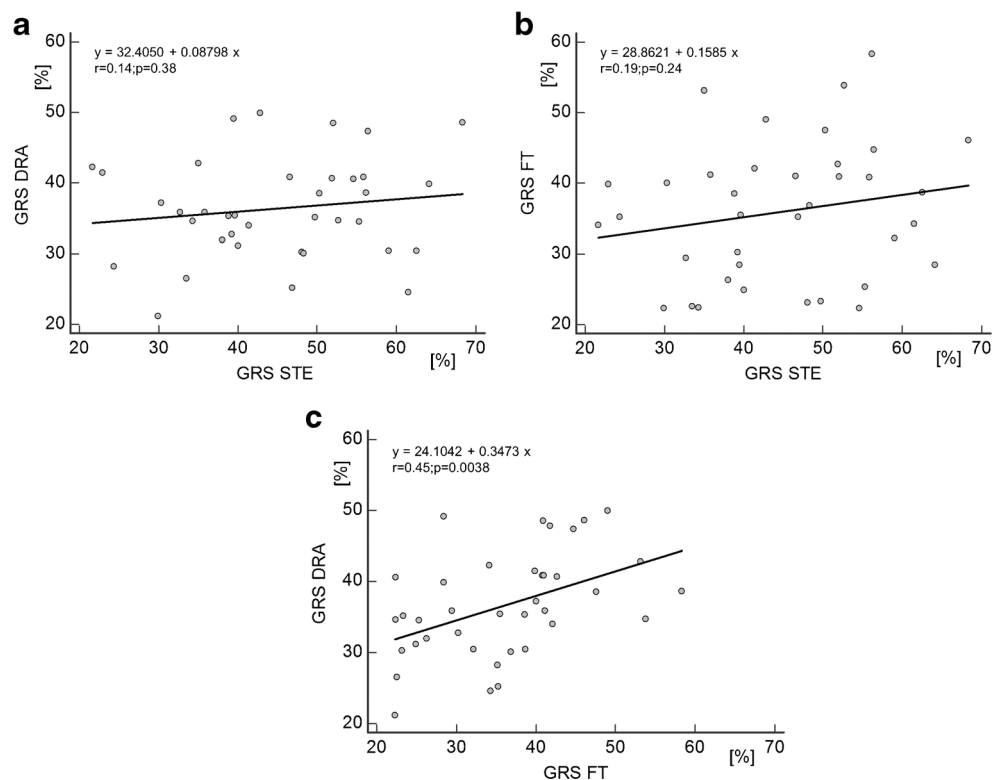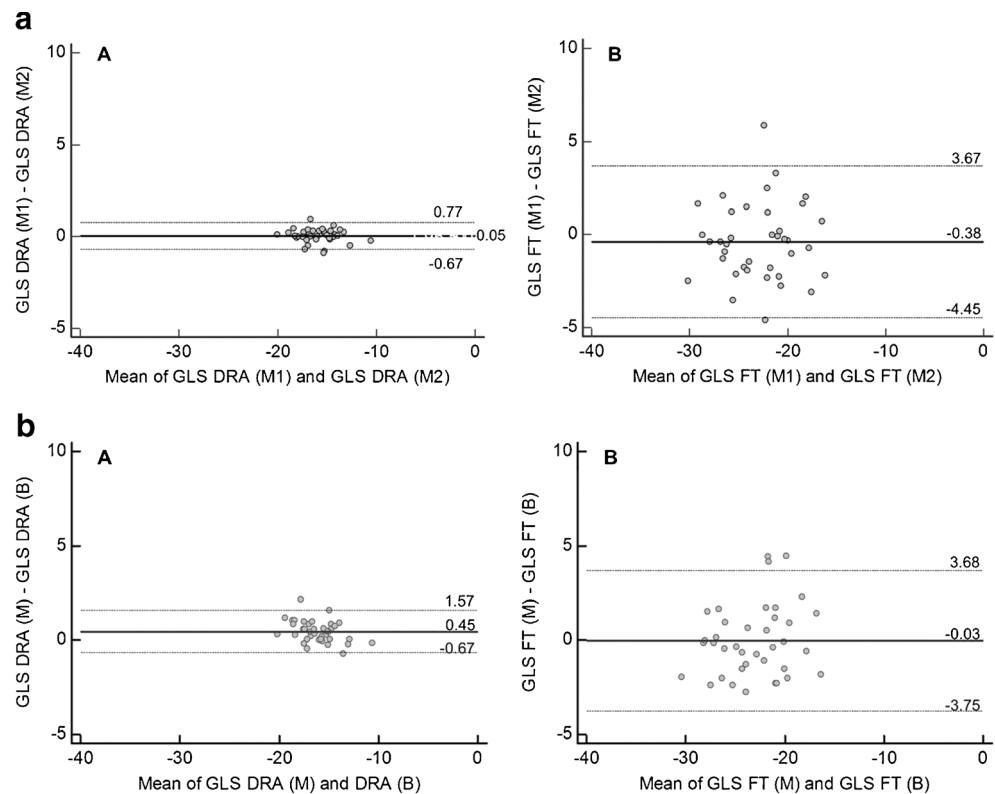
Fig. 7 Bland-Altman plots demonstrating (**a**) intra-observer and (**b**) interobserver agreement for global longitudinal strain (GLS)

good agreement between FT and MR tagging for LV analysis, with a tendency to higher absolute values with FT compared to MR tagging [37, 38]. Moody et al. demonstrated mean values of -19.5±3.5 % and -24.8±2.9 % for FT-derived GLS and GCS while MR tagging-based results were lower at -18.0±3.5 % (p=0.01) and -18.6±2.5 % (p<0.001), respectively [37]. However, as shown in previous studies, correlation between

FT and STE is fairly inconsistent, possibly driven by great variability among studies. Differences in measurements between these two techniques can be related to differences in the region of myocardium tracked [39]. Orwat et al. demonstrated only moderate correlation between FT and STE for GLS (ICC=0.57, COV=14.4 %) and poor correlation between both techniques for GCS (ICC=0.15, COV=19.4 %) [40]. The

Table 5 Intra- (A) and interobserver (B) reproducibility in both applied cine MR-based techniques for global longitudinal (GLS), circumferential (GCS) and radial (GRS) strain

		Intra-observer reproducibility		
		GLS	GCS	GRS
A)				
DRA	Intra-class correlation	0.99 (0.98, 0.99)	1.0 (1.0, 1.0)	1.0 (1.0, 1.0)
	Coefficient of variation (%)	1.6	0.0	0.0
	Mean Bias	0.05 (-0.67, 0.77)	0.0 (0.0, 0.0)	0.0 (0.0, 0.0)
FT	Intra-class correlation	0.91 (0.84, 0.95)	0.95 (0.90, 0.97)	0.91 (0.82, 0.95)
	Coefficient of variation (%)	6.4	5.2	11.8
	Mean bias	-0.38 (-4.45, 3.67)	0.41 (-3.73, 4.56)	-1.65 (-13.44, 10.14)
B)				
DRA	Intra-class correlation	0.97 (0.84, 0.98)	1.0 (1.0, 1.0)	1.0 (1.0, 1.0)
	Coefficient of variation (%)	3.2	0.0	0.0
	Mean Bias	0.45 (-0.67, 1.57)	0.0 (0.0, 0.0)	0.0 (0.0, 0.0)
FT	Intra-class correlation	0.92 (0.86, 0.96)	0.93 (0.84, 0.96)	0.72 (0.47, 0.85)
	Coefficient of variation (%)	5.7	6.1	18.9
	Mean Bias	-0.03 (-3.75, 3.68)	1.11 (-3.39, 5.63)	2.01 (-16.23, 20.26)

For ICC data in parenthesis represent 95 % CI intervals; for BA analysis data in parenthesis represent limits of agreement

Fig. 8 Bland-Altman plots demonstrating (**a**) intra-observer and (**b**) interobserver agreement for global circumferential strain (GCS)
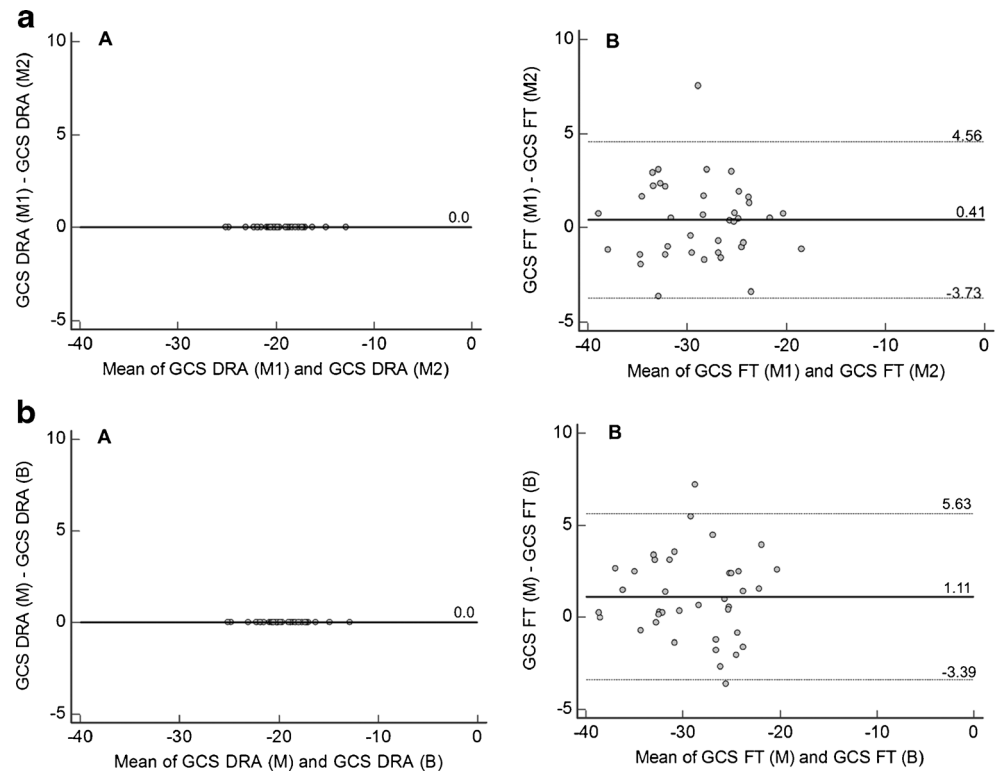
dependency of STE on image quality and acoustic windows for individual segment visualization may further affect results, and have been reported to result in poor agreement between STE and FT in Fontan patients for GLS and GCS (CV 29.9 % and 29.6 %, respectively) [39, 41].

This present study focused on the use of a deformable registration analysis (DRA) tool in combination with automated/semiautomated LV short axis and long axis segmentation, respectively. All phases of a slice are registered to the first phase within this slice and subsequently morphed to the other phases using forward and backward deformation fields. This approach has been shown to result in fast and efficient analysis, with accurate and consistent results [26, 27].

Regarding strain results, we found statistically significant differences between all three methods for GLS and GCS. While FT demonstrated higher absolute values when compared to STE, DRA-derived absolute values were systematically lower when compared to STE. In comparison with STE, higher absolute strain values have previously been reported for FT [21]. Furthermore, for both 2D and 3D STE, higher absolute strain values have been demonstrated in comparison with MR tagging, especially for GLS and GCS [42–44]. Results of presented DRA analysis are within normal ranges of reported MR tagging data [31, 37, 38, 45]. This may in part explain the significant differences between STE and DRA results, although a direct comparison with MR tagging has not been performed in this study. In addition, the differences in haemodynamic status with lower systolic blood pressure and rate-pressure product during the echocardiography study may further contribute to

higher absolute strain values in STE [46]. Despite offsets to STE, no significant differences were identified for global radial strain between FT and DRA analysis.

Besides agreement, reproducibility of quantitative measurements is of high importance in method assessment. Previous studies on feature-tracking reported intra-class correlation coefficients (ICC) of ≥0.85 for intra-observer analysis of all three main strain directions and interobserver analysis of GLS and GCS data [47]. These results are consistent with the results of the present study. Augustine et al. reported coefficients of variation in feature-tracking for GLS, GCS and GRS of 10.9, 4.9, and 32.3 for interobserver and 12.3, 2.8, and 22.9 for intra-observer analysis, respectively. These values were higher for GLS and GRS than reported in the present study but lower for GCS [38].

Direct comparison of long axis DRA and FT data demonstrates superior intra- and interobserver reproducibility for DRA in GLS analysis; perfect reproducibility was demonstrated for short axis-derived DRA related to the fully automated segmentation approach. Even for GLS the robust DRA segmentation approach most likely is a major contributor to the superior reproducibility by significantly eliminating user interaction and bias.

Despite the high reproducibility of DRA-based strain analysis, the partial lack of significant correlation between both MR-based approaches to STE is of concern with respect to the overall rating of these techniques. As described in detail, DRA GLS demonstrated significant correlation with respective STE results after removal of two highly influential data points. For FT, however, correlation remained non-significant even after further data analysis while good correlation between both MR

techniques was consistent. The combination of the above findings may propose general modality/acquisition differences between echo and MRI in addition to different underlying principles of 'tissue tracking' and strain data evaluation [26, 39, 41]. Although the interval between both examinations (echo, MRI) was short (<6 h), interval variation in haemodynamics may have contributed to differences as described (Table 1). In previously published studies comparing FT on MR images and STE, very little detail has been presented about potential haemodynamic changes. While differences in temporal resolution may be another underlying reason, applied cine MRI, however, demonstrate a temporal resolution within the range of typical MR tagging studies.

Study limitations

Although comparison of strain data to the current clinical standard of speckle-tracking echocardiography has been performed, MR tagging data was not available in our study population. Secondly, as the focus of this study was the intra-individual comparison of various methods, we included both healthy volunteers and patients into this study. As presented strain results were primarily within normal ranges, the accuracy of DRA could not be explored across a wide range of normal and abnormal strain values.

Conclusions

Deformable registration-based analysis of cine SSFP data is a novel automated method that could allow assessment of myocardial deformation with reduced variability and superior reproducibility compared to MR feature-tracking. As such, DRA may prove to be an excellent tool for added information in clinical scenarios with especially normal global systolic function. Further studies are warranted in order to assess its accuracy in comparison to MR tagging.

Compliance with ethical standards

Conflict of interest The scientific guarantor of this publication is Dr. Bernd J. Wintersperger, MD. The authors of this manuscript declare relationships with the following companies:

Bernd J. Wintersperger, Research support Siemens Healthcare

Bernd J. Wintersperger, Speakers Bureau & Honorarium Siemens Healthcare

Andreas Greiser, Employee Siemens Healthcare GmbH, Erlangen, Germany

Marie-Pierre Jolly, Employee Siemens Healthcare Medical Imaging Technologies, Princeton, NJ, USA

The authors state that this work has not received any funding. One of the authors has significant statistical expertise. Institutional Review Board approval was obtained. Written informed consent was obtained from all subjects (patients) in this study. Some study subjects or cohorts have been previously reported in Hanneman et al. published online in RADIOLOGY (entitled "*Quantification of Myocardial Extracellular Volume Fraction with Cardiac MRI in Thalassemia Major*"; however this study did not include any evaluation of regional all motion/strain analysis by MRI and had the sole focus of tissue level changes assessment). Methodology: retrospective, case-control study, performed at one institution.

References

1. Pagidipati NJ, Gaziano TA (2013) Estimating deaths from cardiovascular disease: a review of global methodologies of mortality measurement. Circulation 127:749–756
2. McMurray JJ, Pfeffer MA (2005) Heart failure. Lancet 365:1877–1889
3. Lloyd-Jones DM, Larson MG, Leip EP et al (2002) Lifetime risk for developing congestive heart failure: the Framingham Heart Study. Circulation 106:3068–3072
4. Varadarajan P, Pai RG (2003) Prognosis of congestive heart failure in patients with normal versus reduced ejection fractions: results from a cohort of 2,258 hospitalized patients. J Card Fail 9:107–112
5. Solomon SD, Anavekar N, Skali H et al (2005) Influence of ejection fraction on cardiovascular outcomes in a broad spectrum of heart failure patients. Circulation 112:3738–3744
6. Pattynama PM, De Roos A, Van der Wall EE, Van Voorthuisen AE (1994) Evaluation of cardiac function with magnetic resonance imaging. Am Heart J 128:595–607
7. Sanderson JE (2007) Heart failure with a normal ejection fraction. Heart 93:155–158
8. Sjoli B, Orn S, Grenne B et al (2009) Comparison of left ventricular ejection fraction and left ventricular global strain as determinants of infarct size in patients with acute myocardial infarction. J Am Soc Echocardiogr 22:1232–1238
9. Smedsrud MK, Pettersen E, Gjesdal O et al (2011) Detection of left ventricular dysfunction by global longitudinal systolic strain in patients with chronic aortic regurgitation. J Am Soc Echocardiogr 24:1253–1259
10. Shehata ML, Cheng S, Osman NF, Bluemke DA, Lima JA (2009) Myocardial tissue tagging with cardiovascular magnetic resonance. J Cardiovasc Magn Reson 11:55
11. Zerhouni EA, Parish DM, Rogers WJ, Yang A, Shapiro EP (1988) Human heart: tagging with MR imaging–a method for noninvasive assessment of myocardial motion. Radiology 169:59–63
12. Young AA, Axel L, Dougherty L, Bogen DK, Parenteau CS (1993) Validation of tagging with MR imaging to estimate material deformation. Radiology 188:101–108
13. Yeon SB, Reichek N, Tallant BA et al (2001) Validation of in vivo myocardial strain measurement by magnetic resonance tagging with sonomicrometry. J Am Coll Cardiol 38:555–561
14. Jiang K, Yu X (2014) Quantification of regional myocardial wall motion by cardiovascular magnetic resonance. Quant Imaging Med Surg 4:345–357
15. Osman NF, Kerwin WS, McVeigh ER, Prince JL (1999) Cardiac motion tracking using CINE harmonic phase (HARP) magnetic resonance imaging. Magn Reson Med 42:1048–1060
16. Kuijer JP, Hofman MB, Zwanenburg JJ, Marcus JT, van Rossum AC, Heethaar RM (2006) DENSE and HARP: two views on the

same technique of phase-based strain imaging. J Magn Reson Imaging 24:1432–1438

17. Onishi T, Saha SK, Ludwig DR et al (2013) Feature tracking measurement of dyssynchrony from cardiovascular magnetic resonance cine acquisitions: comparison with echocardiographic speckle tracking. J Cardiovasc Magn Reson 15:95

18. Kempny A, Fernandez-Jimenez R, Orwat S et al (2012) Quantification of biventricular myocardial function using cardiac magnetic resonance feature tracking, endocardial border delineation and echocardiographic speckle tracking in patients with repaired tetralogy of Fallot and healthy controls. J Cardiovasc Magn Reson 14:32

19. Hor KN, Baumann R, Pedrizzetti G et al (2011) Magnetic resonance derived myocardial strain assessment using feature tracking. J Vis Exp. doi:10.3791/2356

20. Collins JD (2015) Global and regional functional assessment of ischemic heart disease with cardiac MR imaging. Radiol Clin N Am 53:369–395

21. Onishi T, Saha SK, Delgado-Montero A et al (2015) Global longitudinal strain and global circumferential strain by speckle-tracking echocardiography and feature-tracking cardiac magnetic resonance imaging: comparison with left ventricular ejection fraction. J Am Soc Echocardiogr 28:587–596

22. Piehler KM, Wong TC, Puntil KS et al (2013) Free-breathing, motion-corrected late gadolinium enhancement is robust and extends risk stratification to vulnerable patients. Circ Cardiovasc Imaging 6:423–432

23. Ge L, Kino A, Griswold M, Carr JC, Li D (2010) Free-breathing myocardial perfusion MRI using SW-CG-HYPR and motion correction. Magn Reson Med 64:1148–1154

24. Doesch C, Papavassiliu T, Michaely HJ et al (2013) Detection of myocardial ischemia by automated, motion-corrected, color-encoded perfusion maps compared with visual analysis of adenosine stress cardiovascular magnetic resonance imaging at 3 T: a pilot study. Investig Radiol 48:678–686

25. Jolly MP, Guetter C, Lu X, Xue H, Guehring J (2011) Automatic segmentation of the myocardium in cine MR images using deformable registration. Proc Workshop Statistical Atlases and Computational Models of the Heart: Imaging and Modelling Challenges, Toronto, ON

26. Jolly MP, Guetter C, Guehring J (2010) Cardiac segmentation in MR cine data using inverse consistent deformable registrationInternational Symposium of Biomedical Imaging: From Nano to Macro, Rotterdam, pp 484–487

27. Guetter C, Xue H, Chefd'hotel C, Guehring J (2011) Efficient symmetric and inverseconsistent deformable registration through interleaved optimization. IEEE International Symposium on Biomedical Imaging: from nano to macro, Chicago, IL, pp 590–593

28. Hanneman K, Nguyen ET, Thavendiranathan P et al (2016) Quantification of myocardial extracellular volume fraction with cardiac MR imaging in thalassemia major. Radiology 279:720–730

29. Lang RM, Badano LP, Mor-Avi V et al (2015) Recommendations for cardiac chamber quantification by echocardiography in adults: an update from the American Society of Echocardiography and the European Association of Cardiovascular Imaging. J Am Soc Echocardiogr 28(1-39):e14

30. Jolly MP, Guetter C, Lu X, Xue H, Guehring J (2011) Automatic segmentation of the myocardium in cine MR images using deformable registration.Proc Workshop Statistical Atlases and Computational Models of the Heart: Imaging and Modelling Challenges, Toronto, ON, pp 98–108

31. Epstein FH (2007) MRI of left ventricular function. J Nucl Cardiol 14:729–744

32. Pedrizzetti G, Mangual J, Tonti G (2014) On the geometrical relationship between global longitudinal strain and ejection fraction in the evaluation of cardiac contraction. J Biomech 47:746–749

33. Sun JP, Stewart WJ, Yang XS et al (2009) Differentiation of hypertrophic cardiomyopathy and cardiac amyloidosis from other causes of ventricular wall thickening by two-dimensional strain imaging echocardiography. Am J Cardiol 103:411–415

34. Kempny A, Diller GP, Kaleschke G et al (2013) Longitudinal left ventricular 2D strain is superior to ejection fraction in predicting myocardial recovery and symptomatic improvement after aortic valve implantation. Int J Cardiol 167:2239–2243

35. Yingchoncharoen T, Agarwal S, Popovic ZB, Marwick TH (2013) Normal ranges of left ventricular strain: a meta-analysis. J Am Soc Echocardiogr 26:185–191

36. Marwick TH, Leano RL, Brown J et al (2009) Myocardial strain measurement with 2-dimensional speckle-tracking echocardiography: definition of normal range. JACC Cardiovasc Imaging 2:80–84

37. Moody WE, Taylor RJ, Edwards NC et al (2015) Comparison of magnetic resonance feature tracking for systolic and diastolic strain and strain rate calculation with spatial modulation of magnetization imaging analysis. J Magn Reson Imaging 41:1000–1012

38. Augustine D, Lewandowski AJ, Lazdam M et al (2013) Global and regional left ventricular myocardial deformation measures by magnetic resonance feature tracking in healthy volunteers: comparison with tagging and relevance of gender. J Cardiovasc Magn Reson 15:8

39. Claus P, Omar AM, Pedrizzetti G, Sengupta PP, Nagel E (2015) Tissue tracking technology for assessing cardiac mechanics: principles, normal values, and clinical applications. JACC Cardiovasc Imaging 8:1444–1460

40. Orwat S, Kempny A, Diller GP et al (2014) Cardiac magnetic resonance feature tracking: a novel method to assess myocardial strain. Comparison with echocardiographic speckle tracking in healthy volunteers and in patients with left ventricular hypertrophy. Kardiol Pol 72:363–371

41. Schmidt R, Orwat S, Kempny A et al (2014) Value of speckle-tracking echocardiography and MRI-based feature tracking analysis in adult patients after Fontan-type palliation. Congenit Heart Dis 9:397–406

42. Amundsen BH, Crosby J, Steen PA, Torp H, Slordahl SA, Stoylen A (2009) Regional myocardial long-axis strain and strain rate measured by different tissue Doppler and speckle tracking echocardiography methods: a comparison with tagged magnetic resonance imaging. Eur J Echocardiogr 10:229–237

43. Amundsen BH, Helle-Valle T, Edvardsen T et al (2006) Noninvasive myocardial strain measurement by speckle tracking echocardiography: validation against sonomicrometry and tagged magnetic resonance imaging. J Am Coll Cardiol 47:789–793

44. Kleijn SA, Brouwer WP, Aly MF et al (2012) Comparison between three-dimensional speckle-tracking echocardiography and cardiac magnetic resonance imaging for quantification of left ventricular volumes and function. Eur Heart J Cardiovasc Imaging 13:834–839

45. Jeung MY, Germain P, Croisille P, El Ghannudi S, Roy C, Gangi A (2012) Myocardial tagging with MR imaging: overview of normal and pathologic findings. Radiographics 32:1381–1398

46. Donal E, Bergerot C, Thibault H et al (2009) Influence of after load on left ventricular radial and longitudinal systolic functions: a two-dimensional strain imaging study. Eur J Echocardiogr 10:914–921

47. Taylor RJ, Moody WE, Umar F et al (2015) Myocardial strain measurement with feature-tracking cardiovascular magnetic resonance: normal values. Eur Heart J Cardiovasc Imaging 16:871–881